FACULTY OF SCIENCE
UNIVERSITY OF COPENHAGEN

Bachelor Project, Nanoscience

Jens Rix Nikolajsen

Edge States and Contacts in the Quantum Hall Effect

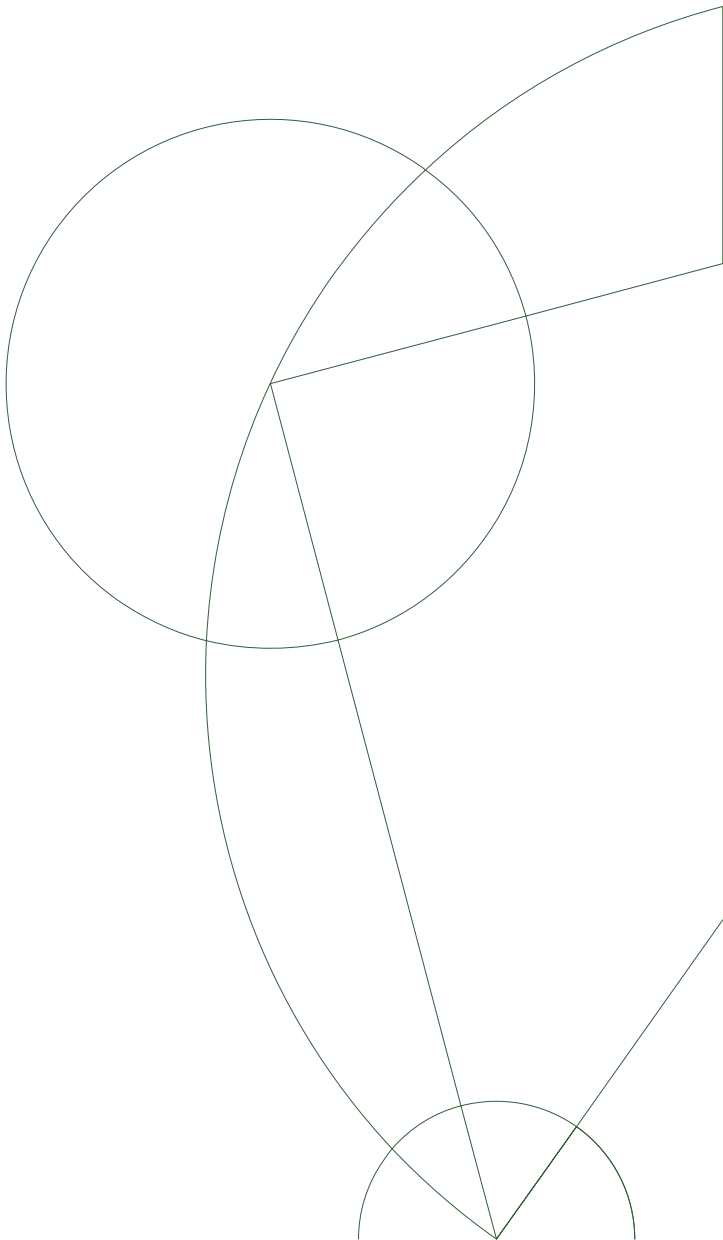

Supervisor: Karsten Flensberg

June 12, 2013

Jens Rix Nikolajsen
050289-XXXX

Nanoscience Center
Niels Bohr Institute
Faculty of Science
University of Copenhagen
Universitetsparken 5
2100 København Ø
Denmark

Resumé

Siden opdagelsen af Kvante Hall effekten i 1980, har emnet været af stor interesse inden for faststoffysikken, og mere end 6000 forskningsartikler er blevet udgivet inden for området. I denne afhandling beskrives de teoretiske aspekter i dette fysiske fænomen, og essentielle elementer som Hall effekten, dannelsen af Landau niveauer, lokalisering af tilstande og tilstedeværelsen af strømbærende kanttilstande bliver gennemgået. Et udtryk for konduktansen i 1-dimensionelle kanaler beregnes ved brug af Landauer-Büttiker formalismen og udtrykket udvides til at beskrive prøver med flere kontakter. Den heltallige kvante Hall effekt undersøges med dette udtryk og den kvantiserede Hall modstand og forsvindende longitudinelle modstand udledes i overensstemmelse med eksperimenter.

Det undersøges, hvordan forskellige kontakter kan påvirke fase kohærente og inkohærente systemer. I det kohærent regime vises det, at den heltallige kvante Hall effekt kan observeres, når nogle kontakter er urene og andre rene, men ikke når alle kontakter er urene. I dekohærente systemer bliver kanttilstandene ækvilibrerede, hvilket medfører, at kontakternes renhed ikke har nogen indvirkning på observationen af den heltallige kvante Hall effekt.

Det beskrives hvordan elektron-elektron vekselvirkninger fører til energigab ved bestemte fraktionelle fyldningsgrader, hvilket er det essentielle i den fraktionelle kvante Hall effekt. Konceptet med strømbærende kantkanaler udvides, så det også gælder i dette regime. Kontakters indvirkning på effekten diskuteres og for tilpas store og rene prøver, hvor både ækvilibrering mellem kanalerne finder sted og hvor alle fraktionelle kanaler forbinder kontakterne, vil der ikke være afvigelser i en FQHE måling.

Abstract

The quantum Hall effect has been a source of great interest ever since its discovery in 1980, and more than 6000 research articles have been published on the topic. In this thesis, the effect is described theoretically starting from the Hall effect, the formation of Landau levels, localization of bulk states and the existence of current carrying edge states. The picture of edge channels is treated using the Landauer-Büttiker formalism from which the conductance of a perfect channel is derived. The expression is expanded in order to describe the multiterminal Hall geometry, and it is used to examine the currents in a integer quantum Hall measurement.

The effect of contact purity is examined in phase coherent and decoherent conductors alike. It is shown that in a phase coherent sample, the integer quantum Hall effect can be observed when some contacts are clean and some are disordered, but it breaks down if all contacts are disordered. In decoherent systems, inelastic scattering equilibrates the edge states in the same way as an ideal contact, and it is proven that disordered contacts have no effect on the quantization in this regime.

It is described how the Coulomb interactions between electrons lead to energy gaps at certain filling factors, which is crucial in the FQHE. The concept of current carrying edge channels is extended, so that it is valid in the fractional regime. The influence of contacts on the FQHE is discussed and for the optimal FQHE measurement a sufficiently large and pure sample should be used, where all fractional channels equilibrate and where the highest filling factor reaches all contacts.

Acknowledgment

Many thanks to Karsten Flensberg for spending hours explaining and discussing with me. Thanks to Anne for care and endless patience during the project and to Jes for thorough proofreading.

Contents

1 Introduction **1**

2 The Hall effect **1**

3 Landau levels **2**
3.1 The quantum mechanical derivation . . . 3
3.2 Broadening of Landau levels . . . 4
3.3 Edge states . . . 5
3.4 Zeeman splitting of the Landau levels . . . 6

4 Landaur-Büttiker formalism **6**
4.1 Two-terminal phase coherent conductance . . . 6
4.1.1 The S-matrix . . . 7
4.1.2 Unitarity of the S-matrix . . . 8
4.1.3 Scattering states . . . 8
4.1.4 The Landauer formula . . . 9
4.2 The quantum point contact . . . 10
4.3 Landauer-Büttiker formalism in multiterminal systems . . . 11

5 The integer quantum Hall effect **12**
5.1 Integer quantum Hall effect in phase coherent conductors . . . 12
5.1.1 Hall geometry with ideal contacts . . . 12
5.1.2 Hall geometry conductor with both ideal and disordered contacts . . . 13
5.1.3 Four terminal conductor with disordered contacts . . . 15
5.2 The quantum Hall effect in macroscopic samples . . . 16
5.3 Limitations in the integer quantum Hall effect . . . 17

6 The experimental observation of the QHE **17**

7 The fractional quantum Hall effect **18**
7.1 Laughlin's wave function . . . 18
7.2 Edge channels in the FQHE . . . 19
7.3 Contact effects in the FQHE . . . 20

8 Conclusion **21**

References **22**

1 Introduction

The study of current carrying samples in magnetic fields has been of increasing interest to the scientific community ever since the discovery of the electromagnetism by H.C. Ørsted in 1820. In 1879, it was observed that a transverse voltage difference builds up, when a conducting sheet is placed in a magnetic field, which is denoted the Hall effect. A century later, quantum oscillations had been observed in similar setups, but in 1980, von Klitzing showed the exact quantization of the Hall resistance at values $\frac{h}{Ne^2}$ for integer N in a 2DEG in strong magnetic fields [1]. The theoretical explanations of the IQHE followed in the years after the experimental observation. Halperin demonstrated that current-carrying edge states played a crucial role [2], and Büttiker calculated the current in these perfect edge channels for multiterminal conductors, and found the quantized values in agreement with the experiments [3][4]. The IQHE is going to play an important role in metrology in the mid 2010s, because it can be used to define the kilogram with great accuracy (according to Klitzing in his Nobel lecture, April 10, 2013).

Only a few years after the discovery of the IQHE, Tsui *et al.* observed plateaus in the Hall resistance at fractional values of N [5]. The theory of the fractional quantum Hall effect was strongly influenced by Laughlin, who pointed out that the Coulomb interactions between electrons played a crucial role, and he came up with a wave function which described the stable fractional states remarkably well. The FQHE has great similarities to the IQHE, and the picture of current carrying edge channels was extended by Beenakker in 1990 [6]. Nobel Prizes have been awarded both for the integer and fractional quantum Hall effects, and research is still being done on the topic.

In this thesis, the fundamental theory needed to verify that the current in the integer quantum Hall effect is carried by edge states is described and the perfect-channel-picture is treated using the Landauer-Büttiker formalism. The effects of the contact purity is discussed in both phase coherent and decoherent regimes. The formation of stable states at certain fractional filling factors in very strong magnetic fields is discussed, and a picture of edge channels valid in this regime is shown. A multiterminal Landauer-Büttiker expression is derived and the contact effects in the FQHE is discussed. The starting point will be the ordinary Hall effect.

2 The Hall effect

When a current carrying sample is placed in a weak magnetic field perpendicular to the current, the moving charges get affected by the Lorentz force. If the current is in the x-direction and the magnetic field in the z-direction, electrons are forced toward the $-$y-direction as shown on figure 1. A charge difference builds up, which causes an electric field in the $-$y-direction, and at some point the force from the electric field on the electrons cancels the Lorentz force. This means that the current will flow in the x-direction in the same way as without a magnetic field, while no current flows in the y-direction. The charge difference gives rise to a transverse Hall voltage V_y (fig. 1).

The effect can be described mathematically using the Drude model, in which electrons in a solid are considered free. The electrons do not feel any Coulomb interactions, and move freely for a collision time τ after which they scatter. When placing such an electron with mass m in an electromagnetic field, the equation of motion reads

$$m\frac{d\boldsymbol{v}_d}{dt} = -e(\boldsymbol{E} + \boldsymbol{v}_d \times \boldsymbol{B}) - \frac{m\boldsymbol{v}_d}{\tau} \ , \tag{2.1}$$

where $\boldsymbol{v}_d$ is the drift velocity. In the stationary state, there is no change in the velocity and for

a two-dimensional system the electric fields are

$$\begin{pmatrix} E_x \\ E_y \end{pmatrix} = \begin{pmatrix} -m/e\tau & -B \\ B & -m/e\tau \end{pmatrix} \begin{pmatrix} v_{d,x} \\ v_{d,y} \end{pmatrix} \tag{2.2}$$

$$= \begin{pmatrix} m/e^2 n_e \tau & B/en_e \\ -B/en_e & m/e^2 n_e \tau \end{pmatrix} \begin{pmatrix} j_x \\ j_y \end{pmatrix} \ , \tag{2.3}$$

where the current density is $\boldsymbol{j} = -en_e \boldsymbol{v}_d$, with n_e being the electron density. As explained, there is no current flowing in the y-direction in the stationary state. The so-called longitudinal and Hall resistivities can be read off from the resistivity tensor in equation 2.3:

$$\rho_{xx} = \frac{m}{e^2 n_e \tau} = \frac{1}{\sigma_0} \ , \tag{2.4}$$

$$\rho_{yx} = -\frac{B}{en_e} \ . \tag{2.5}$$

Thus, there is no magnetoresistivity in the x-direction with resistivity given by the inverse drude conductivity σ_0, while the Hall resistance is proportional to the magnetic field. The constant $R_H = \frac{E_y}{j_x B} = -\frac{1}{en_e}$ is denoted the Hall coefficient. A Hall measurement is used to characterize semiconductor films, as both the electron density n_e and the mobility $\mu = \frac{e\tau}{m}$ can be determined. The Hall effect was discovered by Edwin Hall in 1879, when he did a current/voltage measurement on a rectangular gold sheet placed in a magnetic field [8]. This was about a decade before the Lorentz force was derived, so he could not describe the effect at this point. The experimental observation of the classical Hall effect is seen in the weak magnetic field in figure 9a.

3 Landau levels

As a homogeneous magnetic field only affects electron motion in two dimensions, two dimensional electron gases (2DEG) will be used throughout this thesis. A 2DEG rises experimentally in a heterojunction between a n-type (AlGaAs) and an intrinsic (GaAs) semiconductor. The Fermi energy is between the valence and the conduction bands, but in the junction the conduction band is below Fermi energy. At sufficiently low temperatures, the electrons are in only one particular mode in the direction perpendicular to the junction, thus the electrons are confined to two dimensions.

When a high mobility sample is placed in a strong magnetic field, electrons move in circular orbits due to the Lorentz force. This was not possible in the Hall effect described in the previous section, as the electrons scattered before completing the orbits. A simple classical calculation of the energy of the system can be done, in which it is used that the circumference of the orbit must

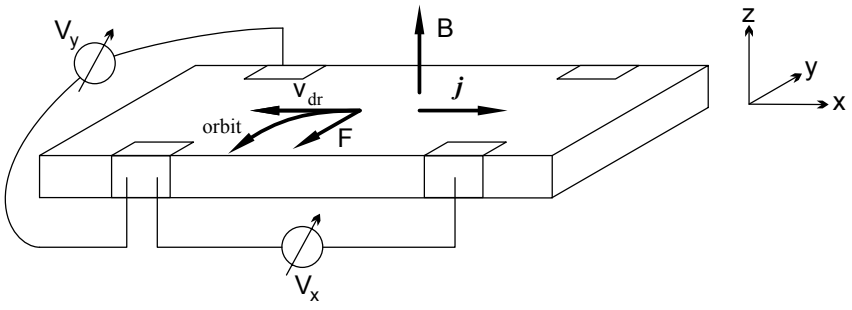

Figure 1: A Hall measurement with current flowing in the x-direction in a magnetic field in the z-direction. The moving electrons are forced to one side of the sample due to the Lorentz force so that a transverse voltage difference V_y builds up, depending on the strength of the magnetic field. From [7].

be equal to an integer n times the wavelength ($n\lambda = n\frac{h}{mv} = 2\pi r_c$). By using that the velocity is $v = r_c\omega_c$ where ω_c is the cyclotron frequency, the kinetic energy is found to be $E = \frac{1}{2}n\hbar\omega_c$. This calculation illustrates that the continuous energy turns into discrete energy levels, but to get the correct result the problem has to be treated quantum mechanically (the quantum mechanical derivation is done with inspiration from [9][7]).

3.1 The quantum mechanical derivation

For electrons in a magnetic field, the Lorentz force is incorporated into the Hamiltonian by replacing the canonical momentum $\boldsymbol{p}$ with the kinetic momentum $\boldsymbol{p} + e\boldsymbol{A}$, where $\boldsymbol{A}$ is the vector potential. The magnetic field is given by the curl of the vector potential ($\boldsymbol{B} = \boldsymbol{\nabla} \times \boldsymbol{A}$). Considering free noninteracting electrons in a magnetic field

$$\frac{1}{2m}\left(\frac{\hbar}{i}\boldsymbol{\nabla} + e\boldsymbol{A}\right)^2 \psi(\boldsymbol{r}) = \varepsilon\psi(\boldsymbol{r}) \ . \tag{3.1}$$

For a magnetic field in the z-direction, different vector potentials can be chosen, e.g. the Landau gauge $\boldsymbol{A} = B_0(0, x, 0)$ and the symmetric gauge $\boldsymbol{A} = \frac{1}{2}B_0(-y, x, 0)$. Here the Landau gauge is used, and for a two dimensional system the Hamiltonian becomes

$$\mathcal{H} = \frac{p_x^2}{2m} + \frac{(p_y + exB_0)^2}{2m} \tag{3.2}$$

$$= \frac{p_x^2}{2m} + \frac{p_y^2}{2m} + \frac{1}{2}m\omega_c^2 x^2 + p_y\omega_c x \ , \tag{3.3}$$

where $\omega_c = \frac{eB_0}{m}$ is the cyclotron frequency. By using that the wave function is that of a free particle in the y-direction

$$\psi(x, y) = u(x)e^{ik_y y} \ , \tag{3.4}$$

the energy can be found in the following way:

$$\mathcal{H}\psi = e^{ik_y y}\left(\frac{p_x^2}{2m} + \frac{\hbar^2 k_y^2}{2m} + \frac{1}{2}m\omega_c^2 x^2 + \hbar k_y\omega_c x\right)u(x) = \varepsilon u(x)e^{ik_y y} \ , \tag{3.5}$$

$$\left(\frac{p_x^2}{2m} + \frac{1}{2}m\omega_c^2\left(x + l_0^2 k_y\right)^2\right)u(x) = \varepsilon u(x) \ , \tag{3.6}$$

where $l_0 = \sqrt{\frac{\hbar}{m\omega_c}}$ is the magnetic length. Equation (3.6) is recognized as the Schrödinger equation for a one dimensional harmonic oscillator with frequency ω_c centered around $x_0 = -l_0^2 k_y$. Thus, the energy of electrons become discrete in a magnetic field with values

$$\varepsilon_n = \left(n + \tfrac{1}{2}\right)\hbar\omega_c \ , \tag{3.7}$$

where $n = 0, 1, 2...$ In 1930, Lev Landau was the first to derive this expression for quantized energy steps using the symmetric gauge [10]. The energy levels are therefore known as *Landau levels*. The electrons which had energies in the interval $[0; \hbar\omega_c]$ without the magnetic field collapses into the the lowest Landau level $n = 0$. The electrons in the energy interval $[\hbar\omega; 2\hbar\omega_c]$ collapses into the next Landau level $n = 1$ and so on. As the magnetic field is increased, more and more electrons collapses into each LL, because $\omega_c = \frac{eB}{m}$. The degeneracy of each LL can be determined from the allowed values of k_y and in the above described picture, the degree of degeneracy is the number of harmonic oscillators with the same quantum number n but with different locations, as $x_0 = -\frac{\hbar}{m\omega_c}k_y$. Since the location of the oscillators has to be inside the sample $0 < x_0 < L_x$ the k_y-values have to fulfill the inequality $-\frac{m\omega_c}{\hbar}L_x < k_y < 0$. Using

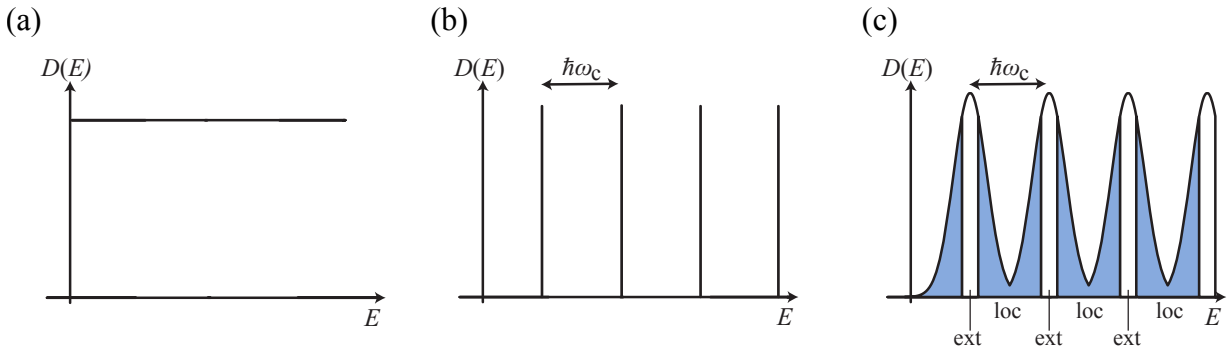

Figure 2: The density of states of electrons in zero magnetic field (a) and in a magnetic field without (b) and with (c) disorder. In (c), the states around half filling factor are extended, while the states around integer filling factor are localized. (c) is from [11].

periodic boundary conditions, each k_y-value take the space $2\pi/L_y$ and the number of states in each Landau level n_L per unit area is

$$n_L = \frac{1}{\mathcal{A}} \frac{m\omega_c}{\hbar} L_x \left(\frac{2\pi}{L_y}\right)^{-1} = \frac{eB}{h} \ . \tag{3.8}$$

To keep track of the number of filled Landau levels, the filling factor ν is introduced

$$\nu = \frac{n_e}{n_L} = \frac{hn_e}{eB} \ , \tag{3.9}$$

where n_e is the electron density. When the filling factor is an integer i, the i lowest Landau levels are completely filled, while the higher Landau levels are all empty. Notice that the filling factor depends both on the magnetic field and the electron density, which means that it can be altered experimentally in two ways.

The density of states $D(E, B)$ for the described system of free electrons is shown for $B = 0$ and in a fixed finite magnetic field in fig 2a and 2b respectively. The density of states is given by

$$D(E, B) = n_L \sum_n \delta(E - \varepsilon_n) \tag{3.10}$$

$$= \frac{eB}{h} \sum_n \delta\left(E - (n + \tfrac{1}{2})\hbar\frac{eB}{m}\right) \ . \tag{3.11}$$

If instead the energy is fixed at the Fermi energy and the magnetic field is changed, the delta peaks appear periodically in 1/B. In the derivation of Landau levels, scattering has been ignored. In the next section, it is discussed that the density of states does not consist of perfect delta peaks when taking the existence of impurities into account.

3.2 Broadening of Landau levels

The sharp delta function in the density of states shown in figure 2b is only valid for pure systems. In a disordered sample, the elastic scattering processes broaden the Landau levels as shown in 2c. The semiclassical explanation is that the trajectories of the electrons that collide with impurities can differ from the perfect orbits as for free electrons. They are therefore allowed to have energies that differ from the Landau levels.

From the above semiclassical consideration, for a model where no edge effects are considered, the electrons in the energy area between two Landau levels are trapped in the vicinity of an impurity. Thus these states are strongly localized in space which, is indicated in figure 2c. The states with energies around the Landau levels are extended which can be shown from computer

simulations [12]. In section 3.3 this will be illustrated, when a potential is added in the derivation of Landau levels and it is shown that states at the edges are extended at all energies.

On increasing the magnetic field at a fixed energy, these broadened peaks in the density of states become further separated and more intense, according to equation (3.11). For sufficiently strong magnetic fields the oscillations in the density of states can be observed in a Hall measurement in both the longitudinal and the transverse resistivities. This is known as the Shubnikov-de Hass effect and it is observed around $0.5T < B < 1.5T$ in the data presented in figure 9 (section 6). The calculation of these oscillations is rather complex and not of interest for the purpose of this thesis, so it will not be described any further.

3.3 Edge states

The importance of edge effects in the description of the integer quantum Hall effect was shown by Halperin in 1982 [2]. This can be demonstrated by adding a potential energy to the Hamiltonian in equation (3.2). Both in the vicinity of impurity atoms and near the edges, there is an increase in the potential energy, which can take shape as illustrated in figure 3a. For strong magnetic fields the cyclotron frequency ω_c becomes large, which means that the harmonic oscillator states are very localized around x_0. For potential energies that vary sufficient slowly, it is therefore reasonable to assume that the potential is constant for each harmonic oscillator $\phi(x) \approx \phi(x_0)$. The addition of the confinement potential in the x-direction gives the energies

$$\varepsilon_n(x_o) = \hbar\omega_c(n + \tfrac{1}{2}) + \phi(x_0) \ . \tag{3.12}$$

The Landau levels therefore get lifted as illustrated in figure 3b, because $x_0 = -\frac{\hbar}{m\omega_c}k_y$. The drift velocity can be found from the slope of the energy dispersion, which gives

$$v_y = \frac{1}{\hbar}\frac{\partial\varepsilon_n(k_y)}{\partial k_y} = -\frac{1}{m\omega_c}\frac{\partial\phi(x)}{\partial x}\Big|_{x=x_0} = -\frac{1}{eB}\frac{\partial\phi(x)}{\partial x}\Big|_{x=x_0} \ . \tag{3.13}$$

Thus the electron velocity is proportional to the negative slope of the potential energy. It is the electrons around the Fermi energy that contribute to the net current, which means that the intersections between the Fermi energy and the dispersions are the points of interest. For the Fermi energy shown in 3b, the bulk states are localized around impurities, which is shown in figure 3c. This agrees with the discussion of localized bulk states in section 3.2. The impurities play a crucial role in the quantum Hall effect, because of this localization. At the edges, the states are extended at all energies. In the situation depicted in fig. 3b, the edges of two Landau levels intersect with the Fermi energy, which means that two edge states can contribute to the conductance. Because of the localized states in the bulk, electrons are not allowed to cross the sample from one edge to the other. As electrons move in the same direction at each edge, this makes it impossible for an electron to backscatter. The above described picture is valid, when the filling factor ν is around an integer number, because the bulk states are localized in this

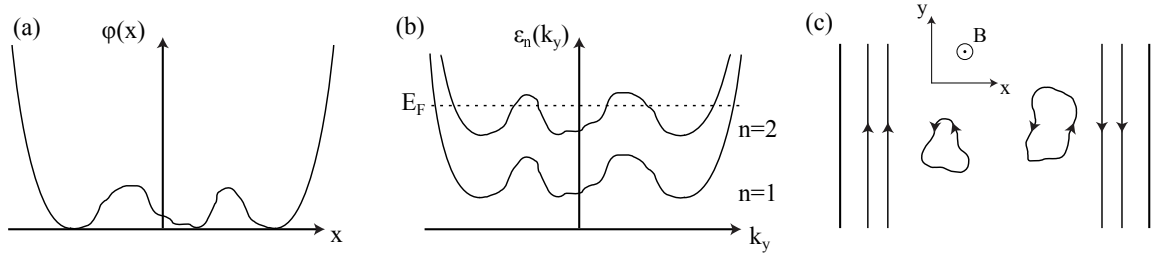

Figure 3: The confinement potential of a disordered sample with a finite size in the x-direction (a). The potential energy is added to the Landau levels in (b), and as the electron velocity is proportional to the negative dispersion slope, the electrons move in space as illustrated in (c). In the bulk, the states are localized around impurities, while they are unidirectional along the edges.

region. In an effort to describe the conductance through these perfect edge channels, which will lead to the integer quantum Hall effect, the Landauer-Büttiker formalism is introduced in the next section.

Around half filling factor (where the Fermi energy is at a Landau level) the states in the bulk overlap, which makes it possible for electrons to cross between the two edges. In other words, the states in the bulk become extended at half filling factor, which is consistent with fig 2c and the explanation in section 3.2. In this regime, the picture of ideal edge channels breaks down.

In the potential depicted in figure 3a, the electrostatic between electrons has been neglected. When taken into account, the potential become more sharp due to the screening effect [13].

3.4 Zeeman splitting of the Landau levels

So far the effect of the electron spin has not been taken into account. Energy levels, which are spin degenerate in zero magnetic field, split up when a magnetic field is applied. Thus, the effect has to be taken into account when discussing the quantum Hall effect. The energies become

$$\varepsilon_{n\sigma} = \left(n + \tfrac{1}{2}\right)\hbar\omega + \phi(x_0) - \tfrac{1}{2}g_e\mu_B B\sigma \ , \tag{3.14}$$

where $\mu_B = \frac{e\hbar}{2m}$ is the Bohr magneton, g_e is the spin g-factor, and $\sigma = \pm 1$ is the spin orientation. When the conductance is derived in the channel picture in section 4 the spin effect is neglected as a starting point, but it is incorporated into the important expressions in the end.

4 Landaur-Büttiker formalism

The picture of current carrying channels can be treated in the Landauer-Büttiker formalism. For simplicity, the starting point will be a two-probe system, which is used to derive the important Landauer formula that describes the conductance in the channel formalism. The two-terminal quantum point contact, in which perfect channels exists, is described in section 4.2 and the Landauer formula is expanded to describe a multiprobe system such as the Hall bar in subsection 4.3. This section is written with great inspiration from [14].

4.1 Two-terminal phase coherent conductance

We will start to examine a mesoscopic region connected by perfect leads to two reservoirs, as shown in figure 4. In a mesoscopic region the inelastic scattering length is longer than the sample size and the transport through the sample is therefore phase-coherent. Electrons coming from reservoir 1 are therefore distributed according to the distribution function of reservoir 1. If these electrons reach reservoir 2, they become equilibrated at the chemical potential and temperature of reservoir 2. This is ensured by using macroscopic conductors as reservoirs, so that the entering electrons scatter inelastically and thereby become equilibrated. By using reflectionless contacts, so that all electrons leaving the mesoscopic region enter the reservoirs, the contacts are denoted clean according to the nomenclature of Büttiker [4]. In sections 5.1.2-5.2 the effects of disorder at a contact is discussed.

The leads in figure 4 are set to be parallel to the x axis, and in the leads the electrons are only allowed to be in an area $\mathcal{A}$ in the y-z plane with impenetrable walls at the boundary. It is therefore a 2-dimensional-particle-in-a-box problem in the z-y plane, which has the solution of plane waves χ_n with corresponding discrete energies ε_n. For lead $\alpha = 1, 2$ the Hamiltonian and the eigenstates read

$$\mathcal{H}_\alpha = \frac{p_x^2}{2m} + \frac{p_\perp^2}{2m}, \qquad \boldsymbol{r}_\perp \in \mathcal{A} \ , \tag{4.1}$$

$$\phi^{\pm}_{\alpha nE}(x, \boldsymbol{r}_\perp) = \sqrt{\frac{m}{2\pi\hbar^2}}\frac{1}{\sqrt{k_n(E)}}\chi_n(\boldsymbol{r}_\perp)e^{\pm ik_n(E)x}, \qquad (x, \boldsymbol{r}_\perp) \in \alpha \ , \tag{4.2}$$

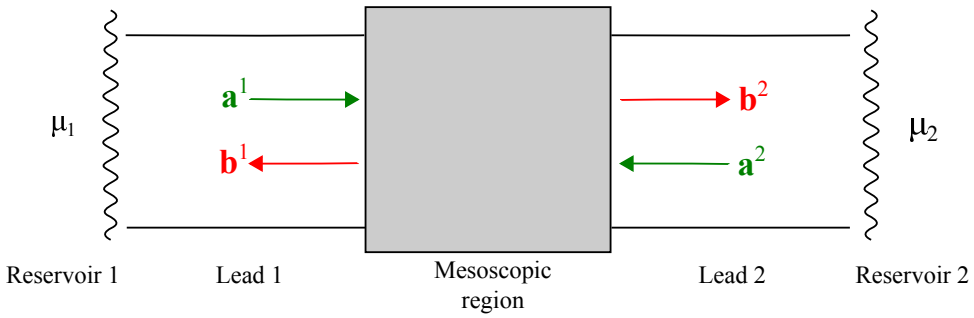

Figure 4: A mesoscopic region is connected to two reflectionless reservoirs at chemical potentials μ_1 and μ_2 by perfect leads. The wavefunction in lead $\alpha = 1, 2$ can be written as a superposition of the incoming and outgoing waves (equation (4.6)) with coefficients $\boldsymbol{a}^\alpha$ and $\boldsymbol{b}^\alpha$ respectively.

where the plus states move to the right and the minus states move to the left both with the wavenumber $k_n(E) = \frac{\sqrt{2m(E-\varepsilon_n)}}{\hbar}$. Each of the eigenstates can carry a current and the positive integer n can therefore be seen as a channel index. An eigenstate with a sufficiently large number $n > M$ is never occupied by an electron, and the lead α is therefore said to have M_α channels.

The eigenstates are normalized in such a way, that they all carry the same current. When an eigenstate is inserted into the current operator, the result has units of current per energy, but when summing up the contributions from more eigenstates, the current unit appears. This is seen by converting the k-sum. A sum over k for eigenstates with the usual normalization $\tilde{\phi_k} = e^{ikx}/\sqrt{\mathcal{L}}$ can be written as $\sum_k \langle\tilde{\phi_k}|A|\tilde{\phi_k}\rangle \to \frac{\mathcal{L}}{2\pi}\int_0^\infty dk \langle\tilde{\phi_k}|A|\tilde{\phi_k}\rangle$. In the chosen normalization, the sum becomes

$$\sum_k \langle\phi_{\alpha nE}|A|\phi_{\alpha nE}\rangle \to \frac{1}{2\pi}\frac{2\pi\hbar^2}{m}\int_0^\infty dk\ k\langle\phi_{\alpha nE}|A|\phi_{\alpha nE}\rangle \tag{4.3}$$

$$= \frac{\hbar^2}{m}\int_0^\infty dE \frac{k}{dE/dk}\langle\phi_{\alpha nE}|A|\phi_{\alpha nE}\rangle \tag{4.4}$$

$$= \int_0^\infty dE \langle\phi_{\alpha nE}|A|\phi_{\alpha nE}\rangle\ . \tag{4.5}$$

This is used in section 4.1.4, when the current is calculated. The states are labeled with E instead of k because of this normalization.

The wavefunctions in lead α can be written as a superposition of the eigenstates (equation (4.2)) with coefficients a_n^α and b_n^α for incoming and outgoing waves respectively where n denotes the channel. At energy E,

$$\psi_E(x, \boldsymbol{r}_\perp) = \begin{cases} \sum_n a_n^1 \phi_{1nE}^+(x, \boldsymbol{r}_\perp) + \sum_n b_n^1 \phi_{1nE}^-(x, \boldsymbol{r}_\perp)\ , & (x, \boldsymbol{r}_\perp) \in \text{ Lead 1}\ , \\ \psi_{\text{MSR},E}(x, \boldsymbol{r}_\perp)\ , & (x, \boldsymbol{r}_\perp) \in \text{ MSR}\ , \\ \sum_n b_n^2 \phi_{2nE}^+(x, \boldsymbol{r}_\perp) + \sum_n a_n^2 \phi_{2nE}^-(x, \boldsymbol{r}_\perp)\ , & (x, \boldsymbol{r}_\perp) \in \text{ Lead 2}\ , \end{cases} \tag{4.6}$$

where MSR denotes the mesoscopic region. The current through the leads is the same as the current through the mesoscopic region, which means that it is not necessary to know the wavefunction $\psi_{Meso,E}(x, \boldsymbol{r}_\perp)$ in order determine the conductance. Instead, the coefficients for the outgoing waves can be related to the coefficients of the incoming waves through the amplitudes of reflection and transmission in this region in the so-called S-matrix.

4.1.1 The S-matrix

Consider an electron that enters the system in figure 4 in the lowest energy channel in the lead 1, $a_1^1 = 1$. In the mesoscopic sample the electron can either be reflected back into lead 1 in the n'th channel with the reflection amplitude r_{n1} or it can be transmitted into the n'th channel in

lead 2 with the amplitude t_{n1}. The equivalent happens if the electron comes from lead 2, where the amplitudes for getting reflected or transmitted from channel n to n' are $r'_{n'n}$ and $t'_{n'n}$. For a simple case with only two channels in each lead, the outgoing coefficients can be determined in the following way

$$\begin{pmatrix} b_1^1 \\ b_2^1 \\ b_1^2 \\ b_2^2 \end{pmatrix} = \begin{pmatrix} r_{11} & r_{12} & t'_{11} & t'_{12} \\ r_{21} & r_{22} & t'_{21} & t'_{22} \\ t_{11} & t_{12} & r'_{11} & r'_{12} \\ t_{21} & t_{22} & r'_{21} & r'_{22} \end{pmatrix} \begin{pmatrix} a_1^1 \\ a_2^1 \\ a_1^2 \\ a_2^2 \end{pmatrix} \quad . \tag{4.7}$$

The 4×4 matrix is called the *scattering matrix* or the *S-matrix*. For the more general case with M channels, the coefficients can be written as vectors, e.g. $\boldsymbol{b^1} = (b_1^1, b_2^1, ..., b_M^1)$ and the S-matrix can be separated into four $M \times M$ submatrices: two reflection matrices $\boldsymbol{r}$ and $\boldsymbol{r'}$ and two transmission matrices $\boldsymbol{t}$ and $\boldsymbol{t'}$.

$$\boldsymbol{c}_{out} = \begin{pmatrix} \boldsymbol{b^1} \\ \boldsymbol{b^2} \end{pmatrix} = \begin{pmatrix} \boldsymbol{r} & \boldsymbol{t'} \\ \boldsymbol{t} & \boldsymbol{r'} \end{pmatrix} \begin{pmatrix} \boldsymbol{a^1} \\ \boldsymbol{a^2} \end{pmatrix} = \boldsymbol{S}\boldsymbol{c}_{in} \tag{4.8}$$

This formalism can be used to define some new states, so-called scattering states, where an incoming coefficient is set to 1 and the outgoing coefficients are found from the S-matrix. These states are described in subsection 4.1.3.

4.1.2 Unitarity of the S-matrix

Due to current conservation, the amount of incoming waves has to equal the amount of outgoing waves. In terms of the coefficients $\sum_n (|b_n^1|^2 + |b_n^2|^2) = \sum_n (|a_n^1|^2 + |a_n^2|^2)$, which can also be written as $\boldsymbol{c}_{out}^\dagger \boldsymbol{c}_{out} = \boldsymbol{c}_{in}^\dagger \boldsymbol{c}_{in}$. On rewriting this quantity in the following way

$$\boldsymbol{c}_{out}^\dagger \boldsymbol{c}_{out} = \boldsymbol{c}_{out}^\dagger \boldsymbol{S} \boldsymbol{c}_{in} = \boldsymbol{c}_{in}^\dagger \boldsymbol{S}^\dagger \boldsymbol{S} \boldsymbol{c}_{in} \ , \tag{4.9}$$

it is seen that $\boldsymbol{S}^\dagger \boldsymbol{S} = \boldsymbol{1}$, which means that the S-matrix is unitary. Writing this out explicitly

$$\boldsymbol{S}^\dagger \boldsymbol{S} = \begin{pmatrix} \boldsymbol{r}^\dagger & \boldsymbol{t}^\dagger \\ \boldsymbol{t'}^\dagger & \boldsymbol{r'}^\dagger \end{pmatrix} \begin{pmatrix} \boldsymbol{r} & \boldsymbol{t'} \\ \boldsymbol{t} & \boldsymbol{r'} \end{pmatrix} = \boldsymbol{1} = \begin{pmatrix} \boldsymbol{r} & \boldsymbol{t'} \\ \boldsymbol{t} & \boldsymbol{r'} \end{pmatrix} \begin{pmatrix} \boldsymbol{r}^\dagger & \boldsymbol{t}^\dagger \\ \boldsymbol{t'}^\dagger & \boldsymbol{r'}^\dagger \end{pmatrix} = \boldsymbol{S}\boldsymbol{S}^\dagger \ , \tag{4.10}$$

it is more easily seen that

$$\boldsymbol{r}^\dagger \boldsymbol{r} + \boldsymbol{t}^\dagger \boldsymbol{t} = \boldsymbol{r}\boldsymbol{r}^\dagger + \boldsymbol{t'}\boldsymbol{t'}^\dagger \ . \tag{4.11}$$

Taking the trace on both sides in equation (4.11) and realizing that the trace can be rewritten in the following way $\mathrm{Tr}[\boldsymbol{r}^\dagger \boldsymbol{r}] = \sum_{nn'} |r_{nn'}|^2 = \mathrm{Tr}[\boldsymbol{r}\boldsymbol{r}^\dagger]$ it is found that

$$\mathrm{Tr}[\boldsymbol{t}^\dagger \boldsymbol{t}] = \mathrm{Tr}[\boldsymbol{t'}^\dagger \boldsymbol{t'}] \ , \tag{4.12}$$

which will be used, when deriving the conductance in section 4.1.4.

4.1.3 Scattering states

In order to determine the conductance through the mesoscopic region it is not necessary to know the particular wavefunction $\psi_{\mathrm{MSR},E}$, but it can be determined from the reflection and transmission coefficients shown in section 4.1.1. A useful way is to introduce states, where only one wave is incoming in lead α in channel n ($a_n^\alpha = 1$). The outgoing coefficients can be found by applying the S-matrix to this state. For a wave incoming in lead 1 in channel n,

$$\psi_{1nE}(x, \boldsymbol{r}_\perp) = \begin{cases} \phi^+_{1nE}(x, \boldsymbol{r}_\perp) + \sum_{n'} r_{n'n} \phi^-_{1n'E}(x, \boldsymbol{r}_\perp) & (x, \boldsymbol{r}_\perp) \in \text{ Lead 1} \\ \sum_{n'} t_{n'n} \phi^+_{2n'E}(x, \boldsymbol{r}_\perp) & (x, \boldsymbol{r}_\perp) \in \text{ Lead 2} \end{cases} \ , \tag{4.13}$$

where the unknown wavefunction $\psi_{\mathrm{MSR},E}(x, \boldsymbol{r}_\perp)$ in the middle region has been excluded. These states are called *scattering states* and for an incoming wave in channel n in lead 2 the scattering state is

$$\psi_{2nE}(x, \boldsymbol{r}_\perp) = \begin{cases} \sum_{n'} t'_{n'n} \phi^-_{1n'E}(x, \boldsymbol{r}_\perp) & (x, \boldsymbol{r}_\perp) \in \text{ Lead 1} \\ \phi^-_{2nE}(x, \boldsymbol{r}_\perp) + \sum_{n'} r'_{n'n} \phi^+_{2n'E}(x, \boldsymbol{r}_\perp) & (x, \boldsymbol{r}_\perp) \in \text{ Lead 2} \end{cases} . \tag{4.14}$$

These scattering states are useful in order to derive the conductance, which is done in the next section.

4.1.4 The Landauer formula

The electric current carried by a wavefunction $\Psi(x, \boldsymbol{r}_\perp)$ through a cross-section $\mathcal{A}$ can be found using the following expression

$$I = -\frac{e\hbar}{2mi} \int_{\mathcal{A}} d\boldsymbol{r}_\perp \left[\Psi^*(x, \boldsymbol{r}_\perp) \Big(\partial_x \Psi(x, \boldsymbol{r}_\perp) \Big) - \Big(\partial_x \Psi^*(x, \boldsymbol{r}_\perp) \Big) \Psi(x, \boldsymbol{r}_\perp) \right] . \tag{4.15}$$

This expression can be derived from the continuity equation. By inserting a scattering state from equation (4.13), the electric current per energy carried by this state can be determined. For an incoming state in channel n in lead 1

$$I_{1nE} = -\frac{e\hbar}{2mi} \int_{\mathcal{A}} d\boldsymbol{r}_\perp [\psi^*_{1nE} (\partial_x \psi_{1nE}) - (\partial_x \psi^*_{1nE}) \psi_{1nE}] \tag{4.16}$$

$$\begin{aligned} &= -\frac{e}{2ih} \int_{\mathcal{A}} d\boldsymbol{r}_\perp \Bigg[\left(\tfrac{1}{\sqrt{k_n}} \chi^*_n e^{-ik_n x} + \sum_{n'} r^*_{n'n} \tfrac{1}{\sqrt{k_{n'}}} \chi^*_{n'} e^{ik_{n'} x} \right) \\ &\qquad \times \left(i\sqrt{k_n} \chi_n e^{ik_n x} - i \sum_{n''} r_{n''n} \sqrt{k_{n''}} \chi_{n''} e^{-ik_{n''} x} \right) \\ &\qquad - \left(-i\sqrt{k_n} \chi^*_n e^{-ik_n x} + i \sum_{n'''} r^*_{n'''n} \sqrt{k_{n'''}} \chi^*_{n'''} e^{ik_{n'''} x} \right) \\ &\qquad \times \left(\tfrac{1}{\sqrt{k_n}} \chi_n e^{ik_n x} + \sum_{n''''} r_{n''''n} \tfrac{1}{\sqrt{k_{n''''}}} \chi_{n''''} e^{-ik_{n''''} x} \right) \Bigg] \end{aligned} \tag{4.17}$$

$$\begin{aligned} &= -\frac{e}{2h} \Bigg[1 - \sum_{n''} \delta_{nn''} r_{n''n} \frac{\sqrt{k_{n''}}}{\sqrt{k_n}} e^{-ik_n x} e^{-ik_{n''} x} + r^*_{nn} e^{2ik_n x} - \sum_{n'} r^*_{n'n} r_{n'n} \\ &\qquad + 1 + r_{nn} e^{-2ik_n x} - r^*_{nn} e^{2ik_n x} - \sum_{n'''} r^*_{n'''n} r_{n'''n} \Bigg] \end{aligned} \tag{4.18}$$

$$= -\frac{e}{h} \left[1 - R^{11}_n \right] = -\frac{e}{h} T^{21}_n . \tag{4.19}$$

where the energy dependence of k_n has been suppressed to simplify the notation. The total probability that the wave incoming in channel n is reflected into any other channel n' in lead 1 is introduced $R^{\alpha\alpha}_n = \sum_{n'} |r_{n'n}|^2$. The amount that is not reflected has to be transmitted and the total transmission probability from lead 1 to lead 2 is introduced T^{21}_n. This transmission probability can also be expressed using the following matrix element $T^{21}_n = (\boldsymbol{t}^\dagger \boldsymbol{t})_{nn}$. From equation (4.17) to (4.18) it is used that the transverse eigenfunctions are orthonomal, so that the integration over $\chi^*_n \chi_{n'}$ gives one when n and n' are equal and zero if they are not equal. For simplicity, the Kronecker's delta has only been written explicitly in one term. The electric current per energy carried by scattering states coming from lead 2 can be derived in the same way, which yields

$$I_{2nE} = \frac{e}{h}\left[1 - R_n^{22}\right] = \frac{e}{h}T_n^{12} \ . \tag{4.20}$$

The total electric current is found by summing up all current contributions from all channels and incoming in both leads and integrating over the energy. In the definition of the scattering states, it is assumed that all incoming waves have the coefficient 1, which means that it is certain that such a state is occupied $|a_n^\alpha|^2 = 1$. As mentioned earlier, electrons incoming from reservoir α are distributed in energy in the same way as in this reservoir. Each current contribution therefore has to be multiplied by the Fermi-Dirac distribution function for the incoming lead. Thus the total electric current is

$$I = -\frac{e}{h}\sum_n \int_0^\infty dE \left[T_n^{21} f(E-\mu_1) - T_n^{12} f(E-\mu_2)\right] \ , \tag{4.21}$$

$$= -\frac{e}{h}\int_0^\infty dE \ \mathrm{Tr}[\boldsymbol{t}^\dagger \boldsymbol{t}]\left[f(E-\mu+eV_1) - f(E-\mu+eV_2)\right] \ . \tag{4.22}$$

Here the expression (4.12) found from the unitarity condition of the S-matrix is used, because $\sum_n T_n^{21} = \sum_n (\boldsymbol{t}^\dagger \boldsymbol{t})_{nn} = \mathrm{Tr}[\boldsymbol{t}^\dagger \boldsymbol{t}] = \mathrm{Tr}[\boldsymbol{t}'^\dagger \boldsymbol{t}']$. The current is now expanded in eV around μ, which is valid for small voltages. It is used that the Fermi-Dirac distribution function becomes a Heaviside step function, which is 1 below and 0 above the Fermi energy, when the temperature is very low. The derivative of the distribution function is therefore a negative Dirac delta function

$$I = -\frac{e}{h}\int_0^\infty dE \ \mathrm{Tr}[\boldsymbol{t}^\dagger \boldsymbol{t}]\frac{\partial f}{\partial E}\Big|_\mu (eV_1 - eV_2) \tag{4.23}$$

$$\overset{T\to 0}{=} \frac{e^2}{h} \ \mathrm{Tr}[\boldsymbol{t}^\dagger \boldsymbol{t}](V_1 - V_2) \ . \tag{4.24}$$

The transmission matrices actually depend on energy, which has been suppressed so far. For sufficiently low temperatures and voltages it is reasonable to assume that they are constant in energy, so that the above integration is valid. The conductance is $G = I/(V_1 - V_2)$, which gives the *Landauer formula*:

$$\boxed{G = \frac{e^2}{h} \ \mathrm{Tr}[\boldsymbol{t}^\dagger \boldsymbol{t}] = \frac{e^2}{h}\sum_n T_n^{21}} \ . \tag{4.25}$$

The spin degree of freedom has not been taken into account so far to keep the notation simple. In order to do so, the trace has to include a trace over the spin orientations; $G = e^2/h \sum_{n\sigma} T_{n\sigma}^{21} = e^2/h \sum_{n\sigma}\sum_{n'\sigma'} |t_{n'n,\sigma'\sigma}|^2$. This just gives twice as many channels with the same factor $\frac{e^2}{h}$ in front. In the quantum point contact, which is discussed in the next section, the states are spin degenerate, so that a factor of 2 appears. Except for the section about the QPC, the spin index will be included in n so that equation (4.25) still holds.

An interesting thing about the Landauer formula is that a perfect channel contributes with $\frac{e^2}{h}$ to the conductance. In order to describe the conductance of the perfect edge channels in the quantum Hall effect, a Landauer-Büttiker formula valid for multiprobe systems is needed. This is derived in section 4.3 but first the quantum point contact, in which perfect channels can be observed, is described.

4.2 The quantum point contact

In 1988, both van Wees *et al.* and Wharam *et al.* measured the conductance through a ballistic 2DEG on top of which they put two gate electrodes [15][16]. The situation is illustrated schematically in figure 5a. By varying the gate voltage in such a setup, the confinement potential of the electrons can be controlled. Without going into any mathematical details, the transverse

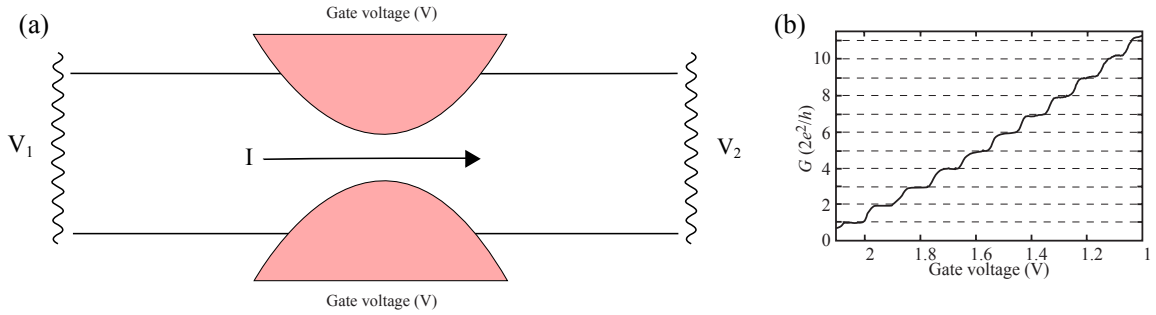

Figure 5: A schematic illustration of a quantum point contact connected to current source and drain at the voltages V_1 and V_2 (a). The conductance through a QPC varies in steps of $\frac{2e^2}{h}$ when changing the gate voltage (b). (b) is reprinted data from [15].

direction in the leads can be thought of as a 1D particle in a box. In the middle region, the gate voltage squishes the hard walls together and thereby the transverse kinetic energies are raised. For a sufficiently large negative gate voltage, none of the electrons coming from the current source (reservoir 1) have enough energy to pass through this middle region. When the gate voltage is reduced, the discrete energy levels of the 1D particle in a box in the middle region are lowered as well. At some point, the lowest energy level ε_1 becomes lower than the energy of the incoming electrons in the middle region, which means that the electrons in this channel have a 100% chance of being transmitted.

The data from van Wees *et al.* is shown in figure 5b, where it is seen that electrons can propagate through the constriction in the lowest channel $n = 1$ with perfect transmission around a gate voltage $V_g = -2,05V$. By varying the gate voltage, the number of available channels can be modified which is the reason for the staircase shape of the data. For N available channels, the conductance is

$$G = \frac{2e^2}{h} N \ . \tag{4.26}$$

Notice the factor of 2, which comes from the spin degeneracy of each channel. It is remarkable to notice that even though the 2DEG is ballistic, there is a resistance $R = \frac{h}{2e^2}$ associated with each channel. This is often called the contact resistance and it can be explained in the following way: An electron coming from the current source does not lose any energy in the QPC, but when it reaches the current drain, it relaxes and thus thermal energy is generated.

4.3 Landauer-Büttiker formalism in multiterminal systems

The derivation of the Landauer formula for multiterminal systems is similar to that of the two probe system. Notice that channels with different spin orientations have different numbers n in this section. The electric currents per energy carried by the scattering states $(\alpha n E)$ and $(\beta \neq \alpha, nE)$ in lead α are given by

$$I^{\alpha}_{\alpha nE} = -\frac{e}{h} \sum_{\beta \neq \alpha} T^{\beta\alpha}_{n} \ , \qquad I^{\alpha}_{\beta nE} = \frac{e}{h} T^{\alpha\beta}_{n} \ . \tag{4.27}$$

The total electrical current in lead α is found by summing up the current contributions multiplied by the distribution functions of the incoming reservoirs

$$I^\alpha = \sum_{\beta n} \int_0^\infty dE\ I^\alpha_{\beta nE}\ f(E-\mu+eV_\beta) \tag{4.28}$$

$$= -\frac{e}{h} \sum_{\beta\neq\alpha,n} \int_0^\infty dE \left[T_n^{\beta\alpha} f(E-\mu+eV_\alpha) - T_n^{\alpha\beta} f(E-\mu+eV_\alpha) \right] \tag{4.29}$$

$$\overset{T\to 0}{=} \frac{e^2}{h} \sum_{\beta\neq\alpha} (T^{\beta\alpha}V_\alpha - T^{\alpha\beta}V_\beta)\ , \tag{4.30}$$

where $T^{\alpha\beta} = \sum_n T_n^{\alpha\beta}$ is the total transmission probability from lead β to α. For the multiprobe system the total transmission probability is not necessarily the same from contact α to β as from β to α, which was the case for the two probe system (see equation (4.12)). In the literature equation (4.30) is often written as

$$I^\alpha = \frac{e^2}{h} \left[(M_\alpha - R^{\alpha\alpha})V_\alpha - \sum_{\beta\neq\alpha} T^{\alpha\beta}V_\beta \right]\ , \tag{4.31}$$

where M_α is the number of channels in lead α and $R^{\alpha\alpha} = \sum_n^M R_n^{\alpha\alpha}$ is the total reflection probability of the incoming waves. Due to current conservation and the fact that no voltage difference between contacts lead to no currents, the following relations appear

$$(M_\alpha - R^{\alpha\alpha}) - \sum_{\beta\neq\alpha} T^{\beta\alpha} = 0 \quad , \quad (M_\alpha - R^{\alpha\alpha}) - \sum_{\beta\neq\alpha} T^{\alpha\beta} = 0\ . \tag{4.32}$$

The formulas presented in this section will be used in the following to describe the currents in a Hall bar.

5 The integer quantum Hall effect

The integer quantum Hall effect arise when using the multiprobe Landauer Büttiker formalism on a system of Hall geometry in the region of integer filling factor, where edges conduct as perfect channels. The effects of decoherence and contact disorder is discussed in order to show that the IQHE can be done with almost no sources of error. The simplest example, which is done in textbooks, is to assume that all contacts in a Hall bar are ideal (e.g. [11]). This will be the starting point.

5.1 Integer quantum Hall effect in phase coherent conductors

5.1.1 Hall geometry with ideal contacts

As mentioned, the simplest example is to assume that all contacts in a Hall measurement are clean as shown in figure 6, where contact 1 is the current source and contact 4 the current drain. There are N edge states available, and for simplicity holes are said to carry the current to avoid confusion with the direction of the electric current. The holes coming from contact 1, equilibrated at the voltage V_1, follow the upper edge as explained earlier with no probability of being scattered to the other edges, and all of them are absorbed into contact 2. As the current from reservoir 1 into a perfect channel is $\frac{e^2}{h}V_1$, the current into the N edge states is $\frac{e^2}{h}NV_1$. Thus, equation (4.30) becomes very simple as $T^{\beta 1} = 0$ for $\beta \neq 2$ and $T^{21} = N$, while the incoming current in contact 1 only comes from contact 6, $T^{16} = N$. In matrix form equation (4.30) for this example is

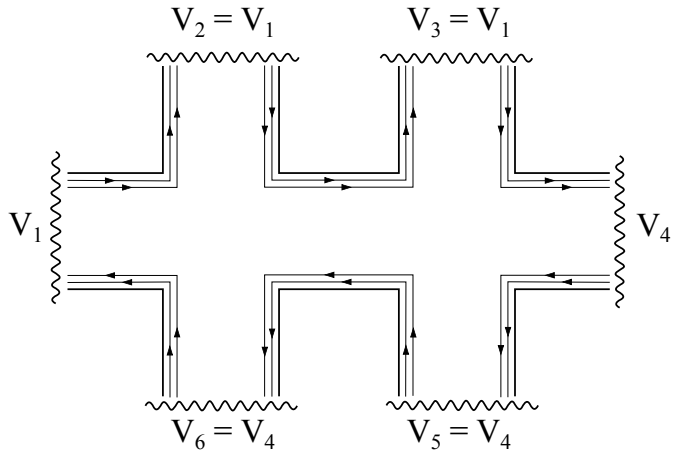

Figure 6: A Hall bar connected to six reservoirs in an ideal manner. The contacts 1 and 4 are considered the current source and drain respectively, while no net current flows in the other contacts. The arrows indicate the direction of the electric current.

$$\begin{pmatrix} I^1 \\ I^2 \\ I^3 \\ I^4 \\ I^5 \\ I^6 \end{pmatrix} = \frac{e^2}{h} \begin{pmatrix} N & 0 & 0 & 0 & 0 & -N \\ -N & N & 0 & 0 & 0 & 0 \\ 0 & -N & N & 0 & 0 & 0 \\ 0 & 0 & -N & N & 0 & 0 \\ 0 & 0 & 0 & -N & N & 0 \\ 0 & 0 & 0 & 0 & -N & N \end{pmatrix} \begin{pmatrix} V_1 \\ V_2 \\ V_3 \\ V_4 \\ V_5 \\ V_6 \end{pmatrix} . \tag{5.1}$$

The total current is $I = I^1 = -I^4 = (e^2/h)N(V_1 - V_4)$. As contact 1 and 4 are current source and drain, there is no current carried by the other contacts, which leads to $V_1 = V_2 = V_3$ and $V_4 = V_5 = V_6$ from (5.1). This means that there is no potential drop between e.g. contacts 2 and 3 and thus there is no longitudinal resistance

$$R_L = R_{14,65} = \frac{V_6 - V_5}{I} = 0 \ , \tag{5.2}$$

where the first two indices (14) in the resistance indicate the current flow and the last two indices (65) indicate where the voltage is measured. The Hall resistance is

$$R_H = R_{14,26} = \frac{V_2 - V_6}{I} = \frac{h}{e^2}\frac{1}{N} \ . \tag{5.3}$$

This spectacular result that the longitudinal resistance disappears and the Hall resistance is quantized around integer filling factors is denoted the integer quantum Hall effect. Experimental results will be shown in section 6. In this simplified textbook example, even the resistance $R_{14,14}$ has the same values as the Hall resistance. The situation becomes more complicated, when all contacts are not considered ideal.

5.1.2 Hall geometry conductor with both ideal and disordered contacts

Following the work done by Büttiker [4], a more complicated situation is now considered where the current source and drain are disordered as shown in figure 7a. It will be shown in section 5.2, that this problem is almost identical to the problem, where all contacts are considered disordered in a macroscopic sample. The problem will therefore be discussed thoroughly.

A disordered contact can be thought of as an ideal contact with a disordered region separating the reservoir and the sample. The contact can be treated in the same way as the two-terminal sample in section 4.1, where the total transmission and reflection probabilities for holes coming from the sample are T_α and R_α. Holes coming from reservoir α have the total probabilities T'_α

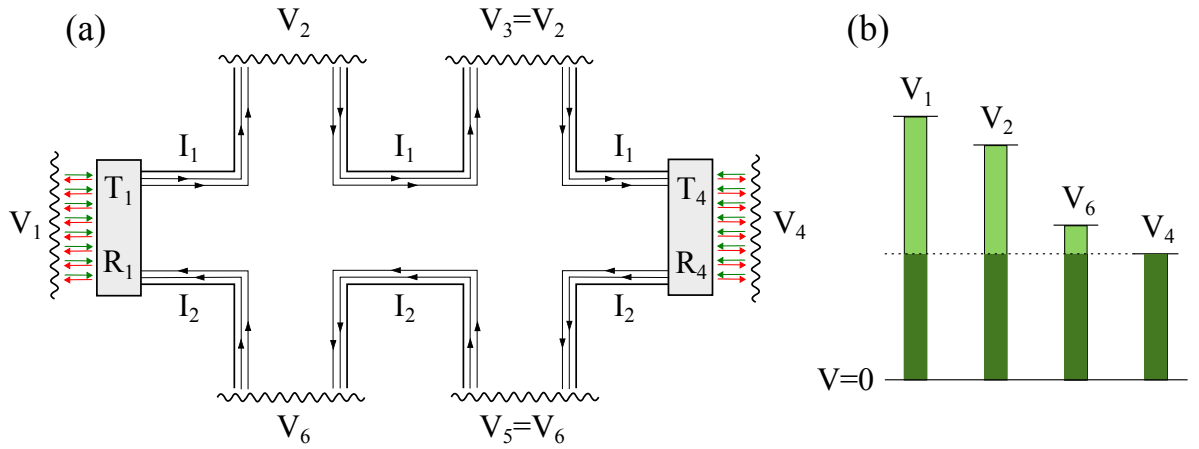

Figure 7: a) A Hall bar with disordered current source and drain (contact 1 and 4 respectively). A current I_1 flows along the upper edge, while a current I_2 flows along the lower edge. b) The currents injected by each reservoir can be expressed using the voltage differences with respect to any voltage of choice. Relative to a zero point, all of the green pillars indicate the currents, while the currents relative to V_4 are light green.

and R'_α. Current conservation requires that $N = T_\alpha + R_\alpha$ and $M_\alpha = T'_\alpha + R'_\alpha$, where N is the number of edge states and M_α is the number of channels in lead α. Due to the condition in eq. (4.12) the two total transmission probabilities are equal $T'_\alpha = T_\alpha$.

Consider first the current I_1 from contact 1 to contact 2 as shown in figure 7a. The holes penetrating the disordered contact from reservoir 1 contributes to this current, but also holes from reservoir 6 that are reflected at contact 1 contribute. Due to the phase coherent transport, the holes maintain the distribution functions of the incoming reservoirs, and thus it does not make sense to talk about an equilibrated chemical potential between these contacts. Reservoir 2 and 3 injects the current I_1 or expressed another way $\frac{e^2}{h}NV_2$ and $\frac{e^2}{h}NV_3$, respectively. Hence the contacts have the same voltage, $V_2 = V_3$. The current along the upper edge is

$$I_1 = \frac{e^2}{h}T_1V_1 + \frac{e^2}{h}R_1V_6 = \frac{e^2}{h}NV_2 \ . \tag{5.4}$$

A similar expression for the current I_2 along the lower edge can be found. Here holes from reservoir 3 and 4 contributes to the current between contact 4 and 5 and because reservoir 5 and 6 injects the same current, $V_5 = V_6$. The current along the lower edge is

$$I_2 = \frac{e^2}{h}R_4V_2 + \frac{e^2}{h}T_4V_4 = \frac{e^2}{h}NV_6 \ . \tag{5.5}$$

Combining equation (5.4) and (5.5), the following expressions for the voltages show up

$$V_2 = V_4 + \frac{NT_1}{N^2 - R_1R_4}(V_1 - V_4) \ , \tag{5.6}$$

$$V_6 = V_4 + \frac{R_4T_1}{N^2 - R_1R_4}(V_1 - V_4) \ . \tag{5.7}$$

To check the result, $T_1 = T_4 = N$ can be inserted which makes the contacts ideal and as expected the result, $V_2 = V_1$ and $V_6 = V_4$, from section 5.1.1 is recovered. If the transmission probabilities are lowered from N, V_2 is lowered as well. The physical interpretation of this is that a larger amount holes distributed around a lower voltage V_6 reaches contact 2, which lowers the overall voltage of the reservoir. Similarly V_6 is slightly larger than V_4, which can be explained using the same argumentation. The total current I flowing from reservoir 1 to 4 can be found by adding up the two contributions from equation (5.4) and (5.5).

$$I = I_1 - I_2 = \frac{e^2}{h}N(V_2 - V_6) = \frac{e^2}{h}\frac{NT_1T_4}{N^2 - R_1R_4}(V_1 - V_4) \ . \tag{5.8}$$

From this expression, it is easily seen that the Hall resistance quantized. The longitudinal resistance is 0 as well, but the two-terminal resistance differs from the one found in last section.

$$R_H = \frac{h}{e^2}\frac{1}{N} \ , \qquad R_L = 0 \ , \qquad R_{14,14} = \frac{h}{e^2}\frac{N^2 - R_1 R_4}{N T_1 T_4} \ . \tag{5.9}$$

Thus the integer quantum Hall effect can be observed in a mesoscopic Hall bar even when the current contacts are disordered.

Another starting point would be to express the current contributions using voltages with respect to the V_4 [4]. The current along the upper edge would then be $I_1 = \frac{e^2}{h}T_1(V_1 - V_4) + \frac{e^2}{h}R_1(V_6 - V_4) = \frac{e^2}{h}N(V_2 - V_4)$ while the current along the lower edge would be $I_2 = \frac{e^2}{h}R_4(V_2 - V_4) = \frac{e^2}{h}N(V_6 - V_4)$. The difference is illustrated schematically in figure 7b, where the light green pillars indicate the current injected by the reservoirs using büttiker's starting point. Of course, the same result appears.

It is remarkable to notice that the current I_2 flows from the current drain to the current source and is proportional to the voltage difference $V_1 - V_4$. The current can be thought of as a circular current that follows the edges around the Hall bar, which is reflected back and forth from contact 1 to contact 4.

As it will be shown in section 5.2, the solution to the problem in figure 7a is the same for a macroscopic sample with disordered contacts. But first it is shown that the integer quantum Hall effect cannot be observed in a mesoscopic sample, when all contacts are disordered.

5.1.3 Four terminal conductor with disordered contacts

In the discussion of a Hall measurement where all contacts are disordered, a four terminal system as shown in figure 8a is chosen to simplify the calculations. This problem is quite more complicated as a hole from a reservoir can reach all other reservoirs. As an example, a hole from reservoir 1 can reach reservoir 4 with the main contribution to the probability $T_1 R_2 R_3 T_4$. Instead of using the transmission and reflection probabilities at each contact, the probabilities $T^{\alpha\beta}$ introduced in equation (4.30) will be used. This general treatment of a four-terminal sample was done by Büttiker in 1986 [3]. As a starting point, equation (4.31) is written in its matrix form

$$\begin{pmatrix} I^1 \\ I^2 \\ I^3 \\ I^4 \end{pmatrix} = \frac{e^2}{h} \begin{pmatrix} M_1 - R^{11} & -T^{12} & -T^{13} & -T^{14} \\ -T^{21} & M_2 - R^{22} & -T^{23} & -T^{24} \\ -T^{31} & -T^{32} & M_3 - R^{33} & -T^{34} \\ -T^{41} & -T^{42} & -T^{43} & M_4 - R^{44} \end{pmatrix} \begin{pmatrix} V_1 \\ V_2 \\ V_3 \\ V_4 \end{pmatrix} \ . \tag{5.10}$$

For the general case where the current flows from contact 1 to 3 and from 2 to 4, the condition $I^1 = -I^3$ leads to

$$(V_3 - V_4) = \frac{T^{12} + T^{32}}{S}(V_2 - V_4) - \frac{T^{41} + T^{21}}{S}(V_1 - V_3) \ , \tag{5.11}$$

$$S = T^{12} + T^{14} + T^{32} + T^{34} = T^{21} + T^{41} + T^{23} + T^{43} \ , \tag{5.12}$$

where the relations (4.32) that each column and row in (5.10) add up to zero have been used. Equation (5.12) can be verified using these relations as well. After a tedious derivation using the relations (4.32) to a great extend, the following expressions for the currents appear

$$\begin{pmatrix} I^1 \\ I^2 \end{pmatrix} = \frac{e^2}{h} \begin{pmatrix} \gamma_{11} & -\gamma_{12} \\ -\gamma_{21} & \gamma_{22} \end{pmatrix} \begin{pmatrix} V_1 - V_3 \\ V_2 - V_4 \end{pmatrix} \ , \tag{5.13}$$

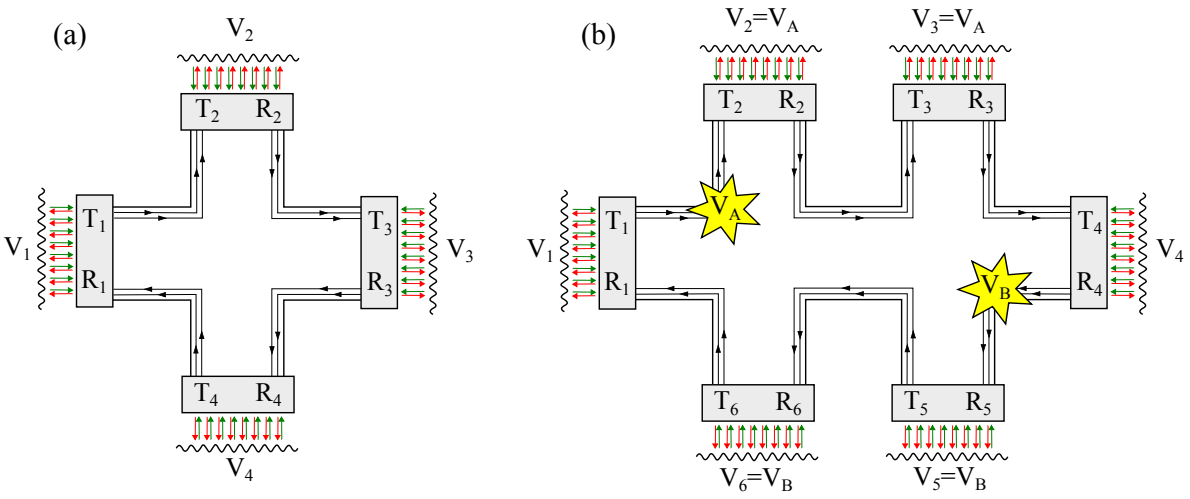

Figure 8: a) A four terminal phase-coherent Hall with disordered contacts. b) A macroscopic Hall bar, in which electrons scatter inelastically when moving from one contact to the other. The inelastic scattering (illustrated by a star) equilibrates the edge states.

where the γ-coefficients are

$$\gamma_{11} = (M_1 - R^{11}) - \frac{(T^{41} + T^{41})(T^{12} + T^{14})}{S} , \tag{5.14}$$

$$\gamma_{12} = \frac{T^{12}T^{34} - T^{32}T^{14}}{S} , \tag{5.15}$$

$$\gamma_{21} = \frac{T^{43}T^{21} - T^{23}T^{41}}{S} , \tag{5.16}$$

$$\gamma_{22} = (M_2 - R^{22}) - \frac{(T^{12} + T^{32})(T^{21} + T^{23})}{S} . \tag{5.17}$$

For a Hall measurement where contact 1 and 3 are current source and drain and the voltage is measured at contact 2 and 4, $I^2 = 0$. The Hall resistance in this setup is

$$R_H = R_{13,24} = \frac{V_2 - V_4}{I^1} = \frac{\gamma_{21}}{\gamma_{11}\gamma_{22} - \gamma_{12}\gamma_{21}} . \tag{5.18}$$

This equation cannot be reduced to the quantized Hall resistance found in the two previous sections, and thus the quantum Hall effect cannot be observed in a phase-coherent conductor with disordered contacts [4].

This general result could have been used to solve the problems in section 5.1.1 and 5.1.2. For a four terminal sample with contact 2 and 4 being ideal and contact 1 and 3 being disordered, the total transmission coefficients would be

$$\begin{pmatrix} M_1 - R^{11} & T^{12} & T^{13} & T^{14} \\ T^{21} & M_2 - R^{22} & T^{23} & T^{24} \\ T^{31} & T^{32} & M_3 - R^{33} & T^{34} \\ T^{41} & T^{42} & T^{43} & M_4 - R^{44} \end{pmatrix} = \begin{pmatrix} T_1 & 0 & 0 & T_1 \\ T_1 & N & 0 & R_1 \\ 0 & T_3 & T_3 & 0 \\ 0 & R_3 & T_3 & N \end{pmatrix} . \tag{5.19}$$

When inserting these coefficients into equation (5.18), the quantized Hall resistance is recovered. The integer quantum Hall effect has now been described thoroughly in phase-coherent conductors. In the next section, the effect of decoherence is described.

5.2 The quantum Hall effect in macroscopic samples

Consider the macroscopic Hall bar in figure 8b, where the distances between the disordered contacts are larger than the inelastic scattering length. In an inelastic scattering event, the edge

states are equilibrated so that e.g. the holes coming from contact 1 and 6 toward contact 2 are equilibrated and distributed at the new voltage V_A [4]. Choosing contact 1 and 4 to be the current source and drain, no net current is leaving the other contacts. A current $\frac{e^2}{h}T_2V_A$ enters contact 2, while the current $\frac{e^2}{h}T_2V_6$ leaves the contact, and since these contributions have to be equal, contact 2 is at the same chemical potential as the phase-randomized incoming holes, $V_2 = V_A$. The same happens at contact 3, and similarly along the lower edge, where the states are equilibrated at the voltage V_B.

From the description given above, it is clear that the inelastic scattering events have the same effect as an ideal contact, which also equilibrates the incoming carriers. In order to find the resistances the macroscopic sample can therefore be treated in the same way as the sample depicted in figure 7a. Thus the equations (5.4)-(5.9) are valid when converting $V_2 \to V_A$ and $V_6 \to V_B$ and the quantized Hall resistance and vanishing longitudinal resistances (eq. 5.9) are recovered.

5.3 Limitations in the integer quantum Hall effect

There are no upper size limit of a Hall bar, in which the integer quantum Hall effect can be observed, but deviations occur if the sample gets too small. For small samples, phase coherence and disordered contacts breaks the effect. Another important thing is that if the edges come to close, electrons can travel from one edge to the other.

Impurities play a crucial role because they localize the bulk states, so that the current is only running on the edges in a large range of magnetic fields. If the sample gets too clean, the plateaus would be shorter. On the other hand, too many impurities can lead to an overlap between the wavefunctions, so that electrons can cross the Hall bar. Quantitatively considerations are complicated, as it both depends on the impurity density, the impurity locations and the shape of the impurity's contribution to the electrostatic potential.

6 The experimental observation of the QHE

The integer quantum Hall effect was observed experimentally by Klaus von Klitzing in 1980 [1], for which he was awarded the Nobel prize. He did a Hall measurement on a 2DEG in a MOSFET (methal-oxide-semiconductor field-effect transistor) in a strong magnetic field of order 15 T. Upon changing the gate voltage and thereby the carrier density, he observed the appearance of plateaus in the Hall resistivity and corresponding disappearance of the the longitudinal resistivity at these points.

The results of a Hall measurement with fixed carrier density but varying magnetic field is shown in figure 9a. At low magnetic field (around $0 < B < 0.4T$), the Hall effect is observed with the resistivities derived from the Drude model (equations (2.4)-(2.5)), while the Shubnikov-de Haas effect is observed in the range around $0.5T < B < 1.5T$. For stronger field, the integer quantum Hall effect is observed with plateaus around integer filling factors at values $\rho_{xy} = \frac{h}{Ne^2} = \frac{25.8k\Omega}{N}$ and corresponding disappearing longitudinal resistivities. At around half filling factors, the bulk states become extended as discussed, which leads to backscattering and breakdown of the perfect channel description. This is seen as a finite longitudinal resistivity and the smeared out Hall steps.

In 1982, Tsui *et at.* observed the existence of plateaus in the hall resistivity and corresponding minima in the longitudinal resistivity at fractional filling factors [5]. The effect which is seen in figure 9b is denoted the fractional quantum Hall effect. For the fractional filling factor $\nu = p/q$, it is seen that q is odd at all plateaus (even denominators have been observed [17]). Around $\nu = 1/2$ great similarities to the integer quantum Hall effect at zero magnetic field show up, which leads to the consideration of new quasiparticles. The theoretical description of the fractional quantum Hall effect is given in the next section, where the edge channel picture is extended.

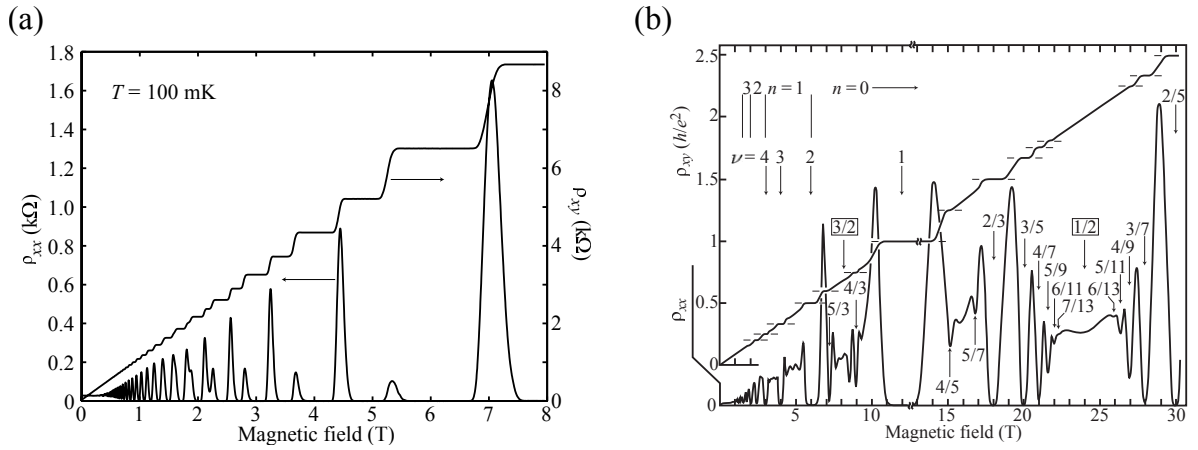

Figure 9: (a) The integer quantum Hall effect observed in a measurement of the longitudinal and Hall resistivities in a GaAs/AlGaAs 2DEG (from [11]). (b) A Hall measurement again in a GaAs/AlGaAs heterostructure in a stronger magnetic field. The formation of Hall plateaus and corresponding minima in the longitudinal resistivity are seen at fractional filling factors (from [17]).

7 The fractional quantum Hall effect

Until this point, electrons have been considered non-interacting, but in order to describe the fractional quantum Hall effect, the Coulomb interactions between electrons have to be taken into account. For sufficiently strong magnetic fields, where the filling factor $\nu < 1$, electrons are in the lowest Landau levels with the same kinetic energy. The kinetic energy is therefore an unimportant factor and the Coulomb interactions become important. By including the electron interaction term in the Hamiltonian, the problem changes from a single-body to a many-body problem.

7.1 Laughlin's wave function

The ground state energy of a two-dimensional system with a few interacting electrons was calculated shortly after the experimental observation of the FQHE [18]. It was found that the internal energy u has a downward cusp at filling factor $\nu = 1/3$. The chemical potential can be thought of as the change in internal energy when adding an electron to the system, and it is given by du/dn. Therefore this cusp leads to a discontinuity in the chemical potential, which implies that the filling factor is constant ($\nu = 1/3$) in some range of chemical potential [19]. In other words, there is an energy gap at $\nu = 1/3$, which means that it is energetically favorable for the system to be at this filling factor. The compressibility, which for an electronic system is $\kappa = (n^2 d\mu/dn)^{-1}$, is zero at this gap and the state is said to be incompressible.

In the same year, Laughlin proposed a ground state wave function, which turned out to describe the interacting electrons at the filling factor $\nu = 1/m$ very well [20]. The wave function has the form

$$\psi_m = \prod_{j<k} (z_j - z_k)^m e^{-\frac{1}{4}\sum_l |z_l|^2} \ , \tag{7.1}$$

where $z_j = x_j + iy_j$ is the coordinate of the j'th electron in complex notation. The prefactor is used to minimize the Coulomb interaction between the electrons by creating a node when the electrons come close to each other. For odd values of m, the interchange of two electrons yields a minus sign, so that the function obeys Fermi statistics. The exponential factors are equivalent to the exponentials in the single-body states of the lowest Landau level (derived using the symmetric gauge in [20]). Laughlin found that it is energetically favorable to be in these states [20], which agrees with both the numeric solution and Monte-Carlo simulations [21].

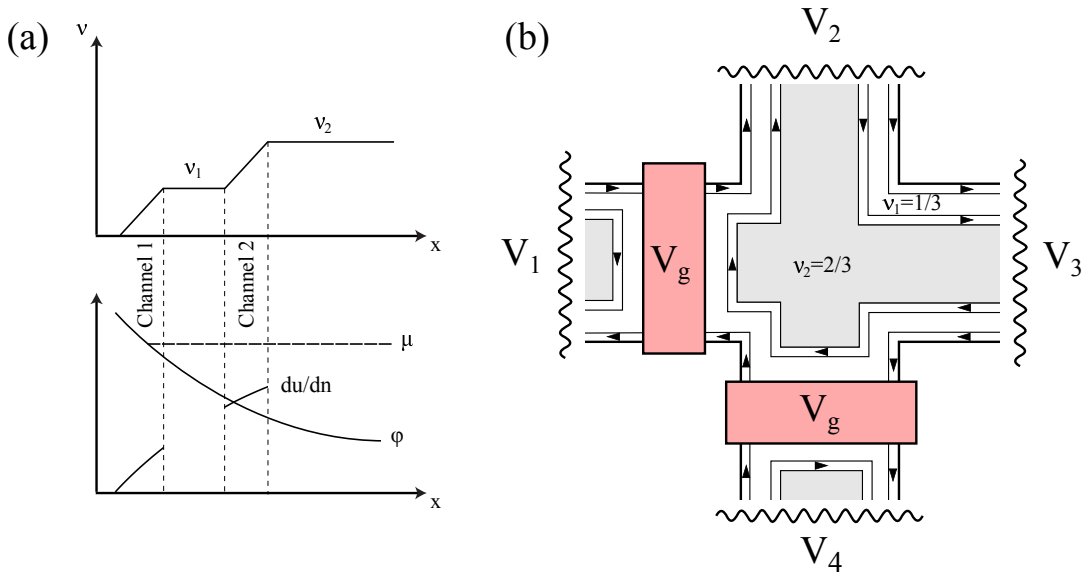

Figure 10: The filling factor ν is lowered when moving from the bulk towards the edges, due to the electrostatic potential ϕ (a). Because of the energy gap in the chemical potential du/dn, incompressible bands form at certain values ν_p. Using gate electrodes the uppermost edge channels can be "turned off". In (b), the channel p=2 is turned off.

Since then it has been found that incompressible states form at a large range of fractional filling factors. In the following only the states $\nu_p = \frac{p}{3}$ will be considered for simplicity.

Because of these energetically favorable states, the filling factor remains constant for some range of magnetic field, which is crucial for the FQHE to be observed. The physical explanation for the pinned filling factor could be that electrons are transferred from a reservoir to change the electron density locally [19].

7.2 Edge channels in the FQHE

In 1990, Beenakker extended the concept of edge channels to the FQHE [6]. Consider a 2DEG conductor as the one shown in a figure 3c placed in a very strong magnetic field, so that the above described theory applies. As the electrostatic potential ϕ is getting stronger at the edges, the electron density drops to zero and so does the filling factor [6]. If the change in ϕ is less than the energy gap associated with a filling factor ν_p within the magnetic length l_0, an incompressible band forms at this value. When moving from the bulk towards the edge, incompressible and compressible states appear alternately as shown in figure 10a. The regions are extended along the edge in the y-direction and they are referred to as bands. As it will be shown in the following, the compressible bands can carry a current, while the incompressible ones cannot.

If the electrochemical potential is raised by $\Delta\mu$ in one end of the conductor, the electron density is changed by

$$\Delta n = \left.\frac{\delta n}{\delta \mu}\right|_{\phi} \Delta\mu = -\left.\frac{\delta n}{\delta \phi}\right|_{\mu} \Delta\mu \ , \tag{7.2}$$

where it is used that the electrochemical potential is $\mu = du/dn + \phi$. The net current density is driven by these electrons, $j = -e\Delta n v_d$, where the drift velocity in the y-direction is proportional to the slope of the electrostatic potential as found in (3.13). By insertion the following current density is found

$$j = -\frac{e}{h}\Delta\mu \frac{\partial \nu}{\partial x} \ , \tag{7.3}$$

where the expression for the filling factor (eq. (3.9)) has been used. Only in the compressible bands, ν changes with x and hence only these bands contribute to the current. By integrating over one compressible band in x, the current carried by this is $I_p = \frac{e}{h}\Delta\mu(\nu_p - \nu_{p-1})$. The total current through this two-terminal conductor is found by summing up the current carried by all compressible edge channels, and the conductance is

$$G = \frac{e}{\Delta\mu}\sum_{p=1}^{P} I_p = \frac{e^2}{h}\sum_{p=1}^{P}\Delta\nu_p \ . \tag{7.4}$$

If $\Delta\nu_p = 1$ for all p, the picture of perfect edge channels in a two-terminal system is recovered (equation 4.25 for $T_n^{21} = 1$). Notice that the different channels can carry different amounts of current, depending on the size of $\Delta\nu_p$. The expression can be expanded to a multiterminal sample. The incoming current $\frac{e^2}{h}\nu_\alpha V_\alpha$ in lead α can either be reflected or transmitted into any other reservoir and hence the current can be expressed in the following way

$$I_\alpha = \frac{e^2}{h}\sum_{\beta\neq\alpha}\left(T^{\beta\alpha}V_\alpha - T^{\alpha\beta}V_\beta\right) \ , \tag{7.5}$$

where the total transmission probability from reservoir α to β is $T^{\beta\alpha} = \sum_{p=1}^{P_\alpha} T_p^{\beta\alpha}\Delta\nu_p$, in which $T_p^{\beta\alpha}$ is the probability that the current injected in the p'th edge channel in α will reach β. Again, if $\Delta\nu_p = 1$ for all p, the multiterminal Landauer-Büttiker formula (4.30) is recovered.

In my opinion, Beenakker exaggerates the importance of the separated incompressible and compressible bands [6]. If an impurity is placed near the edge, the steep increase in electrostatic potential exceeds the energy gap over a magnetic length, so that the imcompressible band collapses. Two compressible bands therefore become adjacent to each other, which allows for scattering between the channels to happen [22]. This does not break down the FQHE. The crucial thing for the effect to be observed is instead that the filling factor is pinned at certain values in the middle regions.

7.3 Contact effects in the FQHE

It has been shown, that the edge channels can be restricted in some regions by changing the filling factor locally, which verifies Beenakker's edge channel picture. This was done by Kouwenhoven *et al.*, who placed gate electrodes across some of the contacts, as shown schematically in figure 10b, in order to lower the electron density [23]. They showed that the uppermost channels p could be turned off, $T_p = 0$, at a particular voltage, indicating that the local filling factor underneath the gate changed to $p-1$. In figure 10b, the uppermost channel, $p = 2$, is restricted from entering contacts 1 and 4, so that it is not contributing to the conductance in a fractional quantum Hall measurement.

In a real FQHE experiment, the low impurity density cannot turn off a channel in the same way as a gate electrode. If the current injected in the p'th channel is not perfectly transmitted to the following reservoir, deviations from the exact fractional quantizations can occur. The discussion whether deviations occur or not is similar to that in section 5.1.2 and 5.2, and it depends on whether scattering between the edge channels happens on the distance between the contacts. If this scattering occurs, the edges are equilibrated and the fractional quantum Hall effect can be observed even when some of the current is reflected.

If the contacts are too narrow, so that the filling factor in the bulk does not stretch all the way to the reservoirs, the uppermost plateaus cannot be observed. The reason is that the electrostatic potential suppresses the electron density in the same way as the gate electrode did in the experiment in figure 10b. To sum up, the FQHE can be observed when the sample is so large that carriers are equilibrated between contacts and the highest filling factor stretches to all contacts.

Research is still being done on the topic of edge channels. In a recent work, Venkatachalam *et al.* connects the outermost edge channel to reservoirs by both quantum point contacts and quantum dots [24]. They find that the even though charges are transported downstream, heat can be transported upstream in the edge channel.

8 Conclusion

In this thesis, the energy levels of electrons in a magnetic field was derived and by applying a electrostatic potential, it was shown that bulk states in a sample are localized while states at the edges are extended. This implies that perfect one-dimensional channels carry the current at the edges, and the conductance of such channels was derived. The expression was expanded to describe multiterminal systems and the quantized Hall resistivity and disappearing longitudinal resistivity were found, when the expression was applied to a Hall geometry.

The influence of contact disorder on the quantization was discussed, and it was shown that ideal or both ideal/disordered contacts give perfect quantization in the phase coherent regime. When all contacts are disordered, perfect steps can be observed in phase decoherent samples, while deviations appear in phase coherent samples.

Energy gaps appear at certain fractional filling factors when taking Coulomb interactions between electrons into consideration. The caps cause that the filling factor gets pinned at these values, so that plateaus are observed in the Hall resistivity. For sufficiently large and pure samples, the fractional edge channels reach all contacts and are equilibrated, so that all gaps can be observed. In the other limit, derivations will occur.

References

[1] K. von Klitzing, G. Dorda, and M. Pepper, "New method for high accuracy determination of fine structure constant based on quantised hall resistance," *Physical Review Letters*, vol. 45, p. 494, 1980.

[2] B. Halperin, "Quantized hall conductance, current-carrying edge states, and the existence of extended states in a two-dimensional disordered potential," *Physical Review B*, vol. 25, no. 4, pp. 2185–2190, 1982.

[3] M. Buttiker, "Four-terminal phase-coherent conductance," *Physical Review Letters*, vol. 57, no. 14, pp. 1761–1764, 1986.

[4] M. Buttiker, "Absence of backscattering in the quantum hall-effect in multiprobe conductors," *Physical Review B*, vol. 38, no. 14, pp. 9375–9389, 1988.

[5] D. Tsui, H. Stormer, and A. Gossard, "Two-dimensional magnetotransport in the extreme quantum limit," *Physical Review Letters*, vol. 48, no. 22, pp. 1559–1562, 1982.

[6] C. Beenakker, "Edge channels for the fractional quantum hall-effect," *Physical Review Letters*, vol. 64, no. 2, pp. 216–219, 1990.

[7] J. Solyom, *Fundamentals of the Physics of Solids*. 2007.

[8] E. H. Hall, "On a new action of the magnet on electric currents," *American Journal of Mathematics*, vol. 2, pp. 287–292, 1879.

[9] L. Landau and E. Lifshitz, *Quantum Mechanics*. Pergamon Press, 1977.

[10] L. Landau, "Diamagnetism of metals," *Zeitschrift fur Physik*, vol. 64, no. 9-10, pp. 629–637, 1930.

[11] T. Ihn, *Semiconductor Nanostructures - Quantum States and Electronic Transport*. 1 ed., 2010.

[12] H. Aoki, "Computer-simulation of 2-dimensional disordered electron-systems in strong magnetic-fields," *Journal of Physics C-Solid State Physics*, vol. 10, no. 14, pp. 2583–2593, 1977.

[13] D. Chklovskii, B. Shklovskii, and L. Glazmann, "Electrostatics of edge channels," *Physical Review B*, vol. 46, no. 7, pp. 4026–4034, 1992.

[14] H. Bruus and K. Flensberg, *Many-Body Quantum Theory in Condensed Matter Physics*. Oxford University Press, 2009.

[15] B. van Wees, H. Vanhouten, C. Beenakker, J. Williamson, L. Kouwenhoven, D. Vandermarel, and C. Foxon, "Quantized conductance of point contacts in a two-dimensional electron-gas," *Physical Review Letters*, vol. 60, no. 9, pp. 848–850, 1988.

[16] D. Wharam, T. Thornton, R. Newbury, M. Pepper, H. Ahmed, J. Frost, D. Hsko, D. Peacock, D. Ritchie, and G. Jones, "One-dimensional transport and the quantization of the ballistic resistance," *Journal of Physics C - Solid State Physics*, vol. 21, no. 8, pp. L209–L214, 1988.

[17] R. Willett, J. Eisenstein, H. Stormer, D. Tsui, A. Gossard, and J. English, "Observation of an even-denominator quantum number in the fractional quantum hall-effect," *Physical Review Letters*, vol. 59, no. 15, pp. 1776–1779, 1987.

[18] D. Yoshioka, B. Halperin, and P. Lee, "Ground-state of two-dimensional electrons in strong magnetic-fields and 1/3 quantized hall-effect," *Physical Review Letters*, vol. 50, no. 16, pp. 1219–1222, 1983.

[19] B. Halperin, "Theory of the quantized hall conductance," *Helvetica Physica Acta*, vol. 56, no. 1-3, pp. 75–102, 1983.

[20] R. Laughlin, "Anomalous quantum hall-effect - an incompressible quantum fluid with fractionally charged excitations," *Physical Review Letters*, vol. 50, no. 18, pp. 1395–1398, 1983.

[21] J. M. Caillol, D. Levesque, J. J. Weis, and J. P. Hansen, "A monte-carlo study of the classical two-dimensional one-component plasma," *Journal of Statistical Physics*, vol. 28, no. 2, pp. 325–349, 1982.

[22] C. L. Kane and M. P. A. Fisher, "Contacts and edge-state equilibration in the fractional quantum hall effect," *Physical Review B*, vol. 52, no. 24, pp. 17393–17405, 1995.

[23] L. P. Kouwenhoven, B. J. van Wees, N. C. Vandervaart, C. J. P. M. Harmans, C. E. Timmering, and C. T. Foxon, "Selective-population and detection of edge channels in the fractional quantum hall regime," *Physical Review Letters*, vol. 64, no. 6, pp. 685–688, 1990.

[24] V. Venkatachalam, S. Hart, L. Pfeiffer, K. West, and A. Yacoby, "Local thermometry of neutral modes on the quantum hall edge," *Nature Physics*, vol. 8, no. 9, pp. 676–681, 2012.